

Preparation and Optimization of Porous Regenerated Cellulose Microspheres from Cellulose Tetraethyl-Ammonium/Urea Solution for Adsorption of Cationic Methylene Blue Dye

Feng Xu, and Byoung-Uk Cho *

Porous regenerated cellulose microspheres (RCMs) have attracted increasing attention due to their wide range of applications from medical carriers to environmental remediation. Here, porous RCMs were synthesized for adsorption of cationic methylene blue dye using a simple emulsification–acid coagulation–oven-drying technique after dissolving pulp cellulose with a degree of polymerization (DP) of approximately 1500 in tetraethylammonium hydroxide (TEAOH)/urea solvents at room temperature. The RCMs with controllable size (20 to 224 μm) and high pore volume (8.24 to 10.20 mL/g) were prepared by varying the dosage of the surfactant polyoxyethylene sorbitan monooleate (polysorbate 80). Moreover, the viscosity of the cellulose solution steadily decreased with storage time due to the decrease in cellulose DP, but the effect on the particle size and morphology of RCMs was negligible, which could be advantageous to the scalable production of RCMs. When used as an adsorbent for cationic methylene blue dye removal, it showed high adsorption efficiency (1 h to achieve equilibrium, 24.5 mg/g), stability, recyclability, and reusability.

DOI: 10.15376/biores.18.1.748-766

Keywords: Tetraethylammonium hydroxide; Cellulose microspheres; Emulsification; Adsorption; Methylene blue

Contact information: Department of Paper Science & Engineering, Changgang Institute of Paper Science and Technology, Kangwon National University, Chuncheon, Kangwaon-Do 24341, South Korea;

* Corresponding author: bucho@kangwon.ac.kr

INTRODUCTION

Organic dyes such as methylene blue (MB) are used widely in industries such as printing, dyeing, leather, cosmetics, and textiles (Lapwanit *et al.* 2018). However, the increased discharge of MB effluents is a global concern, which can damage the ecosystem and threaten public health because of its toxicity, carcinogenicity, accumulation, and non-biodegradability (Tang *et al.* 2021). Hence, effective separation and recycling of MB from wastewater before its release into the environment is essential to eliminate pollution. Various techniques have been exploited to remove MB from effluents; some examples of these techniques are chemical treatments such as photocatalytic degradation and chemical coagulation, and physical treatments such as membrane separation and adsorption (Hua *et al.* 2019; Dong *et al.* 2021). Adsorption is an economical and promising approach with low energy consumption, high efficiency, easy operation, and wide applicability (Molla *et al.* 2018; Li *et al.* 2020). Porous absorbents, such as biochar, activated carbon, graphene-

based, and cellulose materials, have been widely applied in purification processes (Liu *et al.* 2019; Tu *et al.* 2021). In this study, an anionic porous absorbent for cationic MB was developed from a chemical pulp containing cellulose as a main component, which is considered as a representative eco-friendly material.

Cellulose is an abundant natural organic biopolymer with an annual production of 10^{12} tons, and it is one of the most promising candidates for the synthesis of biomaterials because of its unique properties such as eco-friendly renewability and biodegradability (Tu *et al.* 2021). Cellulose is used as an excellent raw material to produce well-shaped regenerated biomaterials such as films, filaments, hydrogels, and microspheres, which have been widely applied in packaging, textiles, and water purification (Buchtova *et al.* 2019; Zhang *et al.* 2019). Cellulose microspheres have drawn increased interest in water purification because of their controllable size, abundant hydroxyl groups, high specific surface area, negative charge, and porosity (Druel *et al.* 2020; Xu and Cho 2020).

Generally, three steps—dissolution of cellulose in a specific solvent, shaping it as spheres, and regeneration (solidification)—are involved in the synthesis of cellulose microspheres (Gericke *et al.* 2013). In a recent study, an organic base solvent (quaternary ammonium/phosphonium hydroxide) was used as a novel non-derivatizing solvent for the dissolution of cellulose under mild conditions, demonstrating perfect solubility for lignocellulose (Abe *et al.* 2012). Moreover, the addition of urea to the aforementioned solvent can replace a part of the organic base and further improve the efficiency of cellulose dissolution (Wei *et al.* 2016; Xu and Cho 2020). Although the addition of urea can stabilize the fresh cellulose–TEAOH/urea aqueous solution (Zhang *et al.* 2019), the stability of cellulose solution in long-term storage at room temperature remains a challenge for the consecutive mass production of regenerated cellulose materials with specific shapes such as regenerated microspheres.

Shaping techniques such as dropping, jet-cutting, high-pressure atomization, and emulsification have been combined with a coagulation step and applied to prepare cellulose beads and microspheres (Li *et al.* 2016; Kim *et al.* 2020). The mean size of cellulose beads prepared by using a dropping technique was in the range 0.5 to 4 mm (Gericke *et al.* 2013; Kim *et al.* 2021), which was higher than those prepared by jet-cutting from cellulose–[DBNH][CO₂Et] solution and coagulated in different coagulation baths such as ethanol, water, and isopropanol (0.5 to 0.7 mm) (Druel *et al.* 2018). High-pressure atomization can produce cellulose microparticles with smaller sizes (~ 2 μm) (Wang *et al.* 2014). However, specialized and expensive equipment is required for these production processes. In contrast, the emulsification technique does not require any special equipment, and the obtained cellulose microspheres have a small mean size (~ 10 to 300 μm) (Gericke *et al.* 2013). In the emulsification technique, a cellulose solution is dispersed in a mixture of oil (cyclohexane, hexadecane, and paraffin oil) and surfactants polyoxyethylene sorbitan monooleate (Span 80 and Span 85; herein identified as polysorbate 80 and 85), and further coagulated in acid or butanol under continuous agitation to form the porous microspheres (Suzuki *et al.* 2014; Luo and Zhang 2010). The porous microspheres can be easily sedimented by gravity, and they can be collected by filtration. In addition, due to their porous structure, diffusion would be relatively rapid into the middle of the material. However, only a few studies have reported the use of cellulose–TEAOH/urea solution by the emulsification technique for preparing regenerated cellulose microspheres (RCMs) and demonstrating their properties. In the previous research (Xu and Cho 2020), the authors reported that the RCMs were easily prepared via emulsification-acid coagulation method using cellulose-TEAOH/urea solution and that the structure and particle size of RCMs

could be controlled by varying the stirring time and stirring speed.

The objective of this study was to synthesize porous RCMs from cellulose–TEAOH/urea solution and to evaluate the product by adsorption of cationic methylene blue dye. The effects of factors such as storage time of cellulose solution and surfactant dosage on the physical and chemical properties of the RCMs were also investigated. Shredded hardwood bleached kraft pulp (HwBKP) was used as the starting raw material, and it was dissolved at room temperature in a TEAOH/urea/H₂O. The effects of the storage time of the cellulose solution on the viscosity, DP, and yield of regenerated cellulose were considered to validate the stability and potential of regenerated cellulose microspheres. Furthermore, RCMs were prepared from a ~2.0 wt% cellulose–TEAOH/urea solution via the emulsification technique at various surfactant dosages. Finally, adsorption characteristics of RCMs for cationic methylene blue dye was studied.

EXPERIMENTAL

Materials

Hardwood bleached kraft pulp (HwBKP, α -cellulose \cong 90%, and DP \cong 1700) from eucalyptus were shredded by Pulverisette 19 Universal Cutting Mill (FRITSCH, Germany) and the shredded pulp (S-HwBKP, DP \cong 1500) was used for further dissolution. Tetraethyl ammonium hydroxide (TEAOH, 35 wt% aqueous solution), urea, paraffin oil, polysorbate-80, acetic acid (99.8 wt%), hydrochloric acid (HCl, 0.1 M), sodium hydroxide (NaOH, 0.1 M), and methyl orange (MO), Congo red (CR), and methylene blue (MB) were purchased from Sigma-Aldrich (St. Louis, MO, USA). All chemicals were of analytical grade and used directly.

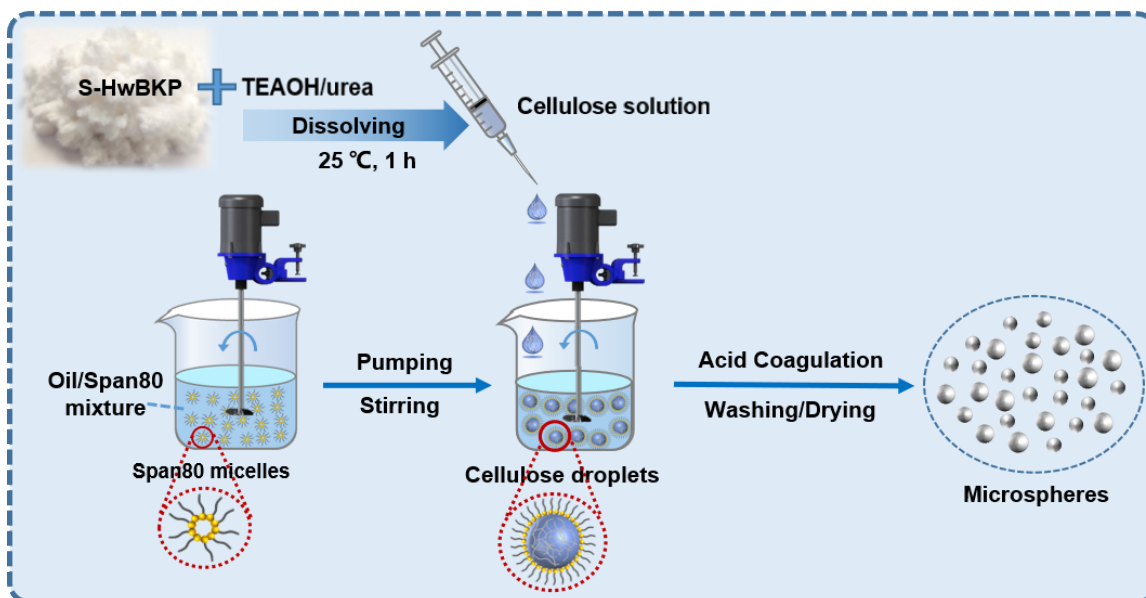


Fig. 1. Procedures for preparation of the RCMs

Preparation of Cellulose–TEAOH/urea/H₂O Solution

TEAOH/urea/H₂O (27/22/51, wt%) solution was prepared using the previously described method (Sirviö and Heiskanen 2019; Xu and Cho 2020). Further, clear and fresh

pulp cellulose–TEAOH/urea/H₂O solutions (~2 wt%) were prepared as follows: 50 g of urea/H₂O in a 100 mL beaker, dried pulp (1.04 g) was added and the mixture was gently stirred for 1 h at 25 °C. Then, the cellulose dispersion mixture was then centrifuged at 8000 rpm (6991 ×g) for 10 min to de-gas and remove the insoluble fraction from the transparent cellulose solution.

Regeneration of Cellulose from Cellulose Solution

To determine a suitable dosage of dilute acetic acid solution for efficiently regenerating RCMs, regeneration of cellulose from cellulose solution was conducted using 10 wt% acetic acid solution at 25 °C. First, 100 g of fresh ~2.0 wt% cellulose solution was prepared. Different amounts (2 to 20 g) of acetic acid solution were added to 50 mL flasks containing 10 g of cellulose solution. The mixture was then stirred at 300 rpm for 3 min, centrifuged at 5000 rpm (2731 ×g) for 5 min. The regenerated cellulose was collected and washed with water until the filtrate became neutral. The pure regenerated cellulose was dried in vacuum for 24 h at 60 °C to further analyze the degree of polymerization (DP) and the regeneration yield. The DP was determined using the equation: $DP^{0.95} = 0.75[\eta]$, where $[\eta]$ is the limiting viscosity of cellulose–copper ethylenediamine (CED) solution. The yield of the regenerated cellulose was calculated using Eq. 1,

$$\text{Regeneration yield} = \frac{m_1}{m_0} \times 100\% \quad (1)$$

where m_0 (0.20 g) is the theoretical dried mass of cellulose in 10 g of cellulose solution and m_1 is the observed dried mass of the regenerated cellulose.

Additionally, regeneration of cellulose from at various storage times was also carried out at 25 °C. Briefly, 10 g of acetic acid solution was added to 50 mL flasks containing 10 g of cellulose solution for different storage times (2 h to 10 days). The separation, washing, and drying procedures, as well as the analysis methods for regeneration yield and DP of regenerated cellulose were the same as those described above.

Preparation of Regenerated Cellulose Microspheres (RCMs)

As shown in Fig. 1, the RCMs were prepared *via* a water-in-oil (W/O) emulsification technique, followed by acid coagulation, which shaped the cellulose solution ('sol') into solid RCMs ('gel') according to a previous study (Xu and Cho 2020). Briefly, cellulose solution was added dropwise to a mixture of paraffin oil and polysorbate 80 using a syringe pump (NE1600, New Era, USA) within 40 min and stirred at 1000 rpm for 4 h. The cellulose solution formed spherical cellulose droplets with the aid of polysorbate 80 in oil. Then, the RCMs were further coagulated using dilute acetic acid solution. The amount of dilute acetic acid solution was optimized by the method described in "Regeneration of Cellulose from Cellulose Solution". The RCMs was washed with deionized water and washed with acetone five times to obtain pure RCMs. Thereafter, the purified RCMs were dried at 60 °C in the oven and then sealed for storage for further adsorption experiments.

Characterization of HwBKP, Cellulose Solutions, and RCMs

Steady shear behavior of the cellulose–TEAOH/urea solutions at different storage time (2 h to 10 day) were studied using a rheometer (HAAKE Viscostester iQ Rheometer, Thermo Fisher Scientific, Germany) equipped with a 40 mm-diameter plate.

The effects of the storage time of cellulose solution (2 h to 10 days) on the regenerated cellulose DP and the yield of regenerated cellulose were studied to validate the stability of the cellulose solution and the potential for RCMs. The dosage of polysorbate 80 was 4 wt% of the weight of paraffin oil. The obtained samples were denoted as RCMs-*i* (*i* = storage time, 1, 3, and 10). The effects of polysorbate 80 dosage in the range 2 to 8 wt% on the cellulose DP, mean size, morphology, and physicochemical properties of the RCMs were further investigated. The obtained samples were denoted as RCMs-*j*% (where *j* = dosage of polysorbate 80).

RCMs were characterized by scanning electron microscopy (SEM, CX-200TM, COXEM, Korea), Fourier-transform infrared spectroscopy (FT-IR, Nicolet Summit, Thermo Fisher Scientific Inc., USA), thermogravimetric analysis (TGA, SDT Q600, TA Instrument, USA), and X-ray diffraction (XRD, Miniflex 600, Rigaku, Japan). The morphology of the RCMs was observed via SEM after spray-coating the samples with gold. The chemical components of S-HwBKP and RCMs, including holocellulose, α -cellulose, low-molecular-weight carbohydrates (hemicellulose and degraded cellulose), lignin, and ash, were measured as previously described (Xu and Cho 2020). The carboxyl content of the samples was determined by the conductometric titration method (Saito and Isogai 2004).

The main physical properties of wet RCMs, such as particle size, swelling ratio (S_r), water content (ω), pore volume (V_p), and porosity (P_r), were determined as follows: The particle size distribution (PSD) and average diameter ($D_v(50)$) of the RCMs were measured using a particle size analyzer (Mastersizer 3000, Malvern, UK). For this measurement, 0.1 g of the dried samples were dispersed in deionized water for 72 h at 25 °C. The S_r values of the RCMs were determined gravimetrically after wiping the excess water from the sample surfaces with moistened qualitative filter paper (Qin *et al.* 2009). The V_p , and P_r values of the wet RCMs were measured via the drainage method, as previously reported (Luo and Zhang 201). The corresponding parameters were calculated using Eq. (2 to 6),

$$S_r = \frac{(W_w - W_d)}{W_d} \quad (2)$$

$$\omega = \frac{(W_w - W_d)}{W_w} \times 100\% \quad (3)$$

$$\rho_g = \frac{W_d}{V - (W_w - W_d)/\rho_{H_2O}} \quad (4)$$

$$V_p = \frac{V - W_d/\rho_g}{W_d} \quad (5)$$

$$P_r = \frac{V_p}{V_p + 1/\rho_g} \quad (6)$$

where W_w and W_d are the weights of wet and dried RCMs, respectively; ρ_{H_2O} is the density of water; volume (V) includes that of absorbed water and of the cellulosic backbone of a certain weight in wet RCMs.

Adsorption Experiments

First, the adsorption ability of RCMs for various dyes including methyl orange (MO), Congo red (CR), and methylene blue (MB) was studied in various absorbent dosages. The dried sample was immersed in 20 mL of 100 ppm dyes solution at 20 °C for 3 h. The absorbent dosages were varied from 20 to 80 mg. Then, the effects of adsorption

pH and adsorbent dosage on MB adsorption of the RCMs-5% were studied. In the adsorption pH study, 40 mg of a dried sample was immersed in 20 mL of 100 ppm MB solution at 20 °C for 3 h. The pH of the MB solution was varied from 2.0 to 12.0 by either 0.1 M HCl or 0.1 M NaOH. The absorbance of the diluted MB solutions before and after adsorption were recorded and the corresponding MB concentrations in those solutions were determined. Furthermore, the removal rate of MB in the solution and the adsorption capacity of MB (q_e) were investigated. The removal rate and q_e were calculated using Eqs. 7 and 8, respectively,

$$\text{Removal} = \frac{(C_0 - C_e)}{C_0} \times 100\% \quad (7)$$

$$q_e = \frac{(C_0 - C_e) \times V}{m} \quad (8)$$

where C_0 (mg/L) and C_e (mg/L) are the MB concentrations in the diluted solution before and after adsorption onto RCMs, respectively; V (L) is the volume of the solution; and m (g) is the dried mass of the adsorbent (g). Additionally, the effects of RCM dosages (20 °C, 10 to 200 mg) and temperature (40 mg RCM dosage, 20 to 60 °C) on q_e were investigated using 20 mL of 100 ppm MB solution at pH 7 and calculated using Eq. 8.

Adsorption Kinetics and Adsorption Isothermal Study

To evaluate the adsorption kinetics of MB, 40 mg of the dried RCMs were added to 20 mL of 100 ppm MB solution at pH 7.0 and 20 °C, and the mixture was stirred continuously; samples were taken at varying adsorption times (5 to 480 min). To study the adsorption isothermal behavior of MB, 40 mg of the dried RCMs were immersed in 20 mL of MB solution with concentrations ranging from 10 to 200 ppm. The adsorption experiments were performed at 20 °C and pH 7.0 for 2 h.

The corresponding adsorption parameters were fitted to pseudo-first-order kinetic (Eq. 9), pseudo-second-order kinetic (Eq. 10), and intra-particle diffusion (Eq. 11) models,

$$\ln(q_e - q_t) = \ln q_e - k_1 t \quad (9)$$

$$\frac{t}{q_t} = \frac{1}{(k_2 q_e^2)} + \frac{t}{q_e} \quad (10)$$

$$q_t = k_3 t^{0.5} + C \quad (11)$$

where q_t (mg/g) is the adsorption capacity at time t , q_e (mg/g) is the equilibrium adsorption capacity, and k_1 (min^{-1}), k_2 ($\text{g}^2 \cdot \text{mg}^{-2}$), and k_3 ($\text{mg} \cdot \text{g}^{-1} \cdot \text{min}^{-1}$) are the rate constants for the pseudo-first-order, pseudo-second-order, and intra-particle diffusion kinetic models, respectively.

The adsorption isotherm behavior was described by classical models, including the Langmuir (Eq. 12), Freundlich (Eq. 13) and Temkin isotherm models (Eq. 14),

$$\frac{C_e}{q_e} = \frac{C_e}{q_m} + \frac{1}{K_L q_m} \quad (12)$$

$$\ln q_e = \ln K_F + \frac{\ln C_e}{n} \quad (13)$$

$$q_e = A \ln B + A \ln C_e \quad (14)$$

where q_m (mg/g) is the maximum adsorption capacity of the adsorbent; K_L (L/mg) is the binding constant of the Langmuir isotherm equation; K_F (mg/g) is the empirical binding

constant; $1/n$ (L/g) represents the empirical constant of the Freundlich isotherm equation; and A (L/g) and B (mg/L) are empirical constants in Temkin isotherm equation, respectively.

Recyclability Test for RCMs

In one set of adsorption-desorption experiments, 200 mg of RCMs were first added to 20 mL of MB solution (100 ppm) at pH 7.0 for 2 h. Then the MB-loaded RCMs were filtered and washed three times with 0.1 M HCl (Hua *et al.* 2019), washed with water to remove HCl, and then washed with acetone three times to obtain pure RCMs. Thereafter, the purified RCMs were oven-dried at 60 °C for 1 h and reused for adsorption. The adsorption-desorption cycle was conducted ten times to evaluate the recyclability of the RCMs using Eq. 7.

RESULTS AND DISCUSSION

Effect of Storage Time on the Properties of Cellulose Solution and RCMs.

The stability of cellulose solution was verified during long-term storage at room temperature. After 10 days of storage, the cellulose solution was still as clear as the initial solution (Fig. S1). Although the cellulose solution did not change in appearance, the viscosities changed dramatically with the passage of time (Fig. 2a). The obtained cellulose solution exhibited relatively high η values after storage for 2 h (0.083 day) at room temperature. As the storage time was extended, η values of cellulose solution decreased notably. For example, η decreased from 1.41 to 0.41 Pa.s ($\dot{\gamma} = 60 \text{ s}^{-1}$) when the storage time increased from 0.083 day to 10 days. Degradation of cellulose inevitably occurred during the dissolution and regeneration processes in alkaline and acidic solvents, such as NMMO, LiCl/DMAc, and ZnCl₂ (Lu and Shen 2011). Therefore, owing to the high alkalinity of the TEAOH solution (pH>14.0), degradation of pulp components such as cellulose and hemicellulose possibly occurred after dissolution and storage under mild conditions. In addition, a notable shear-thinning behavior was observed in all samples (Fig. 2a), indicating that the cellulose in solution remained in the polymeric form possessing a certain DP after alkaline-cutting or degradation of pulp components.

As shown in Fig. 2b, the obtained cellulose solution was relatively clear when the pH of the cellulose solution was >14.0, because the amount of acetic acid added was insufficient to regenerate cellulose (acetic acid: cellulose solution = 0.2:1). When the mass ratio increased to 0.5:1, a sol-gel transition occurred, and the dissolved cellulose was regenerated with a yield of ~30.0 wt%. Upon further increasing the ratio to 0.8:1, the pH of the mixtures gradually decreased to ~13, and the regeneration yield of cellulose notably increased to ~98.0 wt%. As the acetic acid to cellulose mass ratio increased to 2.0:1, no noticeable change was observed in the regeneration yield of cellulose, except for a continuous decrease in the pH value. Therefore, regulating the pH of the cellulose solution appropriately using an acid solution can efficiently regenerate cellulose. The DP and regeneration yield of the regenerated cellulose at different storage times are shown in Fig. 2c. Interestingly, no changes were observed in the regeneration yield (~98.0 wt%) when the storage time was extended from 2 h to 10 days. However, the average DP of regenerated cellulose gradually decreased from ~1100 to ~650 with increasing storage time. These results indicated that the long chains of cellulose were degraded to shorter chains during

storage in the TEAOH/urea solvent.

The cellulose solution was stable, although the viscosity decreased with increasing storage time owing to cellulose degradation because of the high alkalinity of TEAOH; the cellulose was also efficiently coagulated and regenerated in high yields under acidic conditions. This indicated that using a well-dissolved, stable cellulose solution to regenerate cellulose-based products such as RCMs via the emulsion-coagulation technique can be an important step for subsequent applications such as adsorbents, drug delivery, and biocatalysts. First, the effect of the storage time of the cellulose solution on the formation of RCMs are shown in Fig. 2d–i. The wet RCMs obtained from cellulose solutions having different storage times exhibited a similar particle size distribution (Fig. 2d). The average diameter did not vary significantly ($\sim 170 \mu\text{m}$) because of the constant surface tension (Fig. 2g). The microspheres exhibited similar morphology features such as spherical shapes and rough surfaces, implying that the viscosity of the cellulose solutions did not significantly influence the preparation of microspheres under the same emulsion-coagulation technique.

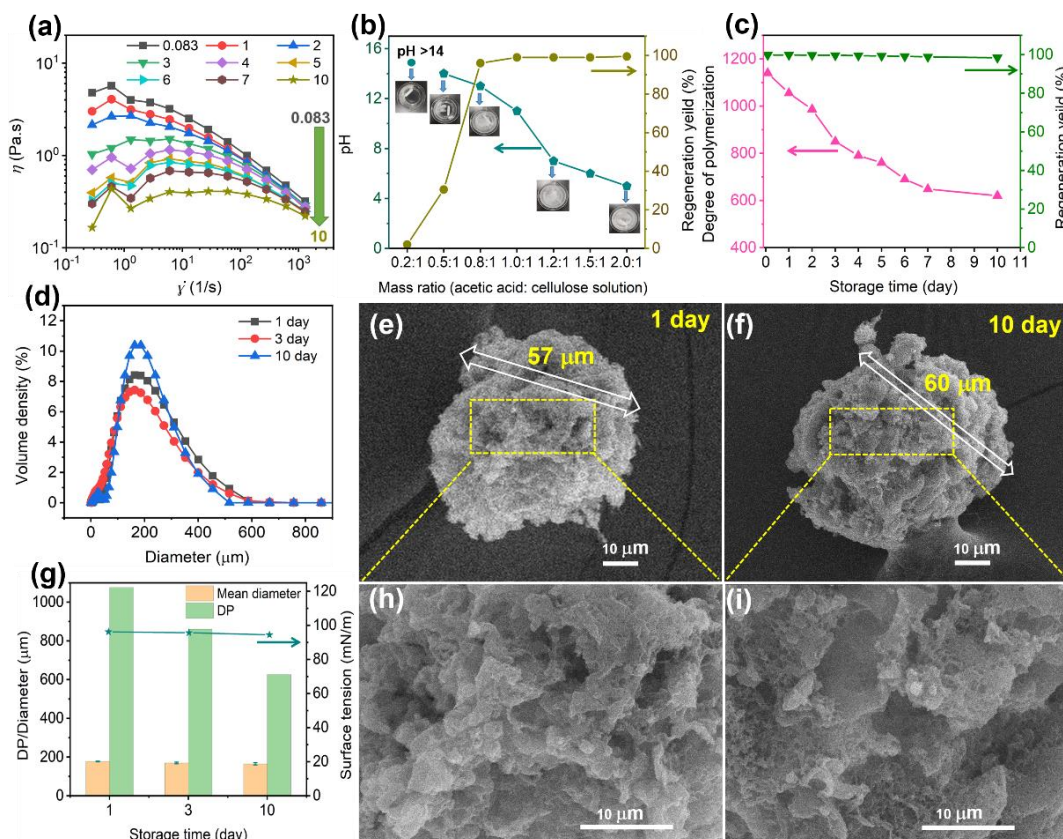


Fig. 2. (a) The apparent viscosity (η) as function of (shear rate) $\dot{\gamma}$ for cellulose solution at different storage time. (b) Effect of mass ratio (acetic acid: cellulose solution) on pH value of the mixture and the regeneration yield of cellulose. (c) Effect of storage time of cellulose solution on the degree of polymerization (DP) and the regeneration yield of cellulose. (d) Effect of storage time on the particle size distribution of obtained RCMs. (g) Effect of storage time on the surface tension of cellulose solution and mean diameter and DP of the obtained RCMs. SEM images of RCM samples obtained from cellulose solution with storage time of (e, h) 1 day and (f, i) 10 day.

Effect of Polysorbate 80 Dosage on the Properties of RCMs

Figure 3a shows the particle size distributions of the wet RCMs produced by varying the amount of surfactant (polysorbate 80). All curves exhibited a normal distribution. The wet microspheres exhibited a relatively narrow distribution range at a higher surfactant dosage (5 to 8 wt% relative to the weight of paraffin oil) than at a lower dosage (2 to 4 wt%), suggesting that a high dosage of polysorbate 80 resulted in high uniformity in the particle sizes. In addition, the mean size of the RCMs could be adjusted by varying the amount of polysorbate 80 (Fig. 3b). The average diameter of the RCMs decreased notably from 267 to 22 μm with an increase in the dosage of polysorbate 80 from 2 to 8 wt%, indicating an approximately 13-fold reduction. The increased amount of polysorbate 80 could decrease the surface tension of the cellulose solution and disperse the cellulose solution in smaller microdroplets into paraffin oil, resulting in smaller particle sizes of the cellulose beads. Additionally, no noticeable change was observed in the cellulose DP (~ 1000) of the RCMs because a cellulose solution within a storage time of 2 days was applied for the fabrication of the RCMs.

Table S1 and Fig. 3c further present the comparison of chemical components and functional groups of S-HwBKP and the RCMs-3%. As shown in Table S1, the RCMs exhibited lower contents of 1% NaOH (2.09%), carboxyl groups (0.07 mmol/g), and lignin (0.65%) than those in HwBKP (3.70%, 0.09 mmol/g, and 0.95%, respectively), indicating that a small part of hemicellulose, cellulose, and lignin could not be regenerated as they were degraded and dissolved in the TEAOH/urea solution. The α -cellulose content (90.15%) in S-HwBKP was lower than that in the RCMs (94.60%), suggesting that the RCMs had higher purity and increased alkali resistance. The aforementioned changes in the chemical properties were further confirmed via ATR-FT-IR spectroscopy. As shown in Fig. 3c, the bands in the region 1000 to 1200 cm^{-1} were characteristic of hemicellulose, which was dominated by the stretching vibrations of the glycosidic linkages (C-O-C) and side groups (C-OH) (Peng *et al.* 2009). In the RCM IR spectra, the absorption bands at 1045 and 1116 cm^{-1} were attenuated, implying a decreased hemicellulose content, which was consistent with the results of the chemical components shown in Table S1. The band at 1336 cm^{-1} , which was characteristic (C-O stretching mode) of the lignin group (syringyl (S) ring), was also weakened, indicating a lower lignin content in the regenerated cellulose. The strong peak at 3320 cm^{-1} , which was ascribed to the stretching vibration of the hydroxyl group ($-\text{OH}$) in the cellulose of HwBKP, shifted to a higher wavenumber (3340 cm^{-1}) in the RCM spectra. In addition, the peaks at 1431 and 896 cm^{-1} were notably shifted to 1420 and 893 cm^{-1} , respectively, implying the transformation of the cellulose crystalline structure from cellulose I to cellulose II (Adsul *et al.* 2012).

The crystalline parameters of the initial HwBKP sheet, shredded HwBKP, and the RCMs-3% were measured via XRD. The corresponding diffraction patterns are shown in Fig. S2a. The initial HwBKP sheet and shredded HwBKP displayed typical cellulose I peaks at $2\theta = 15.2^\circ$, 16.3° , and 22.4° , which were assigned to the (1-10), (110), and (200) planes, respectively. In contrast, the RCMs exhibited typical cellulose II peaks at $2\theta = 12.4^\circ$, 20.0° , and 21.6° (assigned to the (1-10), (110), and (020) planes, respectively) (Xie *et al.* 2020). Thus, the X-ray and FT-IR results indicated a transition of the cellulose crystalline structure from cellulose I to cellulose II during the dissolution and regeneration processes. Additionally, the results of TG and DTG analyses of S-HwBKP and RCMs-3% showed similar thermal decomposition characteristics, indicating that the RCMs had good thermal stability (Fig. S2b).

Table 1 shows the physical properties of the shredded HwBKP and microsphere products (RCMs) having various dosages of polysorbate 80. As expected, RCMs exhibited a high swelling ratio (8.27 to 10.23 g/g), pore volume (8.24 to 10.20 mL/g), and porosity (90 to 93%), which were much higher than those of shredded HwBKP (4.92 g/g, 4.91 mL/g, and 81%, respectively). Moreover, the mean size decreased from 240 to 30 μm , pore volume from 10.20 to 8.24 mL/g, and porosity from 93 to 90%, respectively. The RCMs with a larger mean size exhibited higher pore volume and porosity, possibly because the larger wet RCMs possessed a looser internal porous structure than the smaller ones. Additionally, the high swelling ratio, pore volume, and porosity suggest that the RCMs have hydrophilic and porous characteristics, making them excellent adsorbents for water purification. Additionally, the morphologies of the RCMs synthesized with various amounts of polysorbate 80 (3.0 wt%, Fig. 3d and g; 5.0 wt%, Fig. 3e and h; and 6.0 wt% Fig. 3f and i) in the emulsion process revealed that the microspheres had similar spherical shapes and rough surfaces composed of abundant microporous structures (yellow circles). Notably, the highly networked structures were composed of nanoscale porous structures (red blocks). It was suggested that the micro/nanoporous structures were formed by the entanglement (or interlacing) and overlapping of cellulose during the regeneration process. The small particle size, abundant micro/nanoporous structures, and high porosity favor the effective adsorption and penetration of chemicals into the RCMs during the subsequent adsorption process.

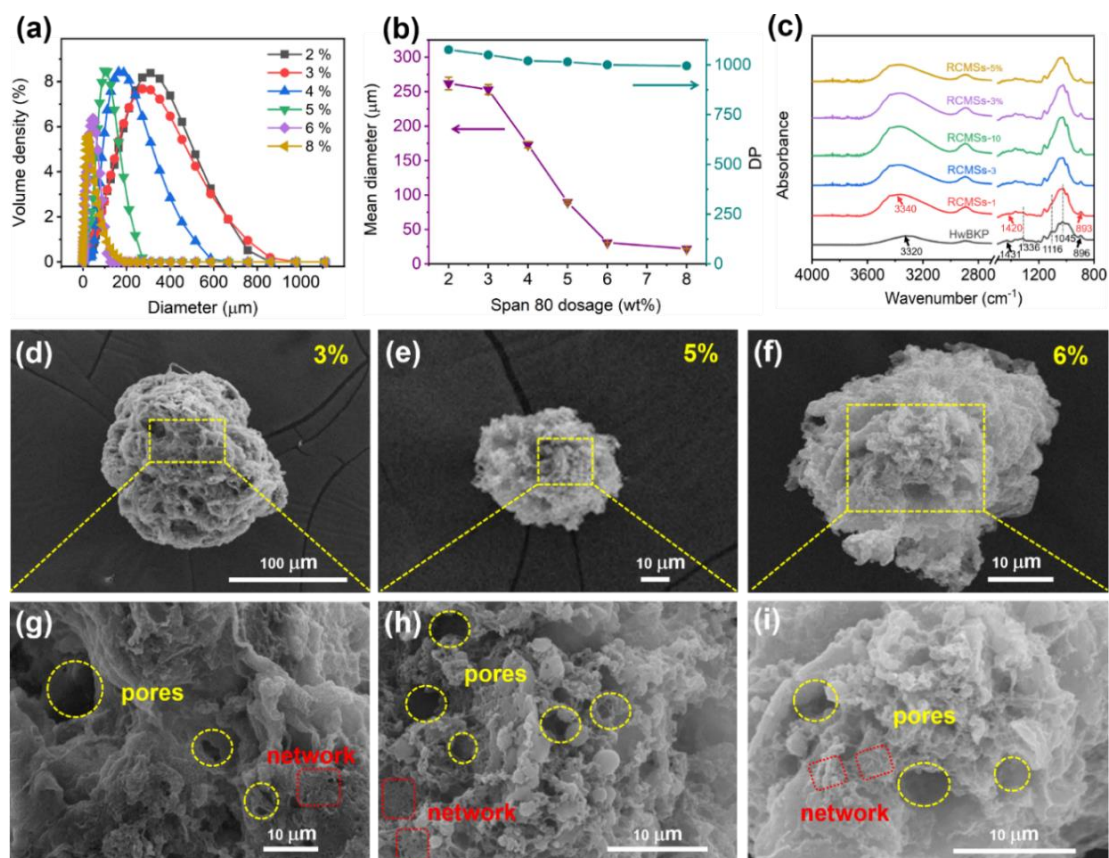


Fig. 3. (a) Effect of polysorbate 80 dosage on the size distribution of obtained RCMs. (b) Effect of polysorbate 80 dosage on the mean diameter and DP of obtained RCMs. (c) FTIR spectra of HwBKP and RCMs. SEM images of RCMs samples obtained at polysorbate 80 dosages of (d, g) 3%, (e, h) 5%, and (f, i) 6%

Table 1. Physical Properties of HwBKP and RCMs

Sample	Mean size (μm)	Swelling ratio (g/g)	Water content (%)	Pore volume (mL/g)	Porosity (%)
S-HwBKP	-	4.92	81.0	4.91	83.0
RCMs-3%	249	10.23	91.0	10.20	93.0
RCMs-5%	89	9.57	91.0	9.54	92.0
RCMs-6%	31	8.27	89.0	8.24	90.0

MB Adsorption Characteristics of RCMs

Firstly, the adsorption ability of RCMs for various dyes including methyl orange (MO), Congo red (CR) and methylene blue (MB) was studied in various absorbent dosages. Herein, MO and CR are anionic dyes containing anionic groups (sulfonic groups, SO_3^-), which have a net anionic charge character when dissolved in deionized water ($\text{pH} \approx 7$). MB is a cationic dye containing a cationic group (S^+) with a net cationic charge characteristic when dissolved in deionized water ($\text{pH} \approx 7$). Obviously, the adsorption capacity of RCMs for MB was higher than for MO and CR under various absorbent dosages (Fig. S3), which could be attributed to the stronger electrostatic attraction between cationic MB and anionic RCMs. Therefore, MB solution was chosen as simulated dye wastewater to further explore the adsorption behavior of RCMs in the following works.

Functional groups such as hydroxyl ($-\text{OH}$) and carboxyl groups ($-\text{COOH}$) in RCMs play a vital role in affecting the adsorption capacity under different pH conditions. The effect of the initial pH of the methylene blue (MB) solution ($\text{pH} = 2.0$ to 12.0) on the adsorption capacity (q_e) of RCMs-5% was investigated. As shown in Fig. 4a, q_e was the lowest under strongly acidic conditions ($\text{pH}=2.0$) owing to the lack of electrostatic attractive force between the uncharged $-\text{OH}$ and $-\text{COOH}$ of the RCMs and cationic MB molecules, which was also confirmed that the RCMs exhibited a nearly neutral charge at $\text{pH} 2.0$ (Fig. 4a). By extending the solution pH to 7.0 , the $-\text{COOH}$ from the surface of the RCMs was gradually deprotonated, the zeta potential decreased to negative values (≈ -22.0 mV, Fig. 4a), and the maximum q_e was obtained because of the strong electrostatic attractive force between the negative surface of the RCMs and cationic MB molecules. As the pH was steadily increased, q_e gradually decreased, possibly resulting from the competition between the excess OH^- ions and MB molecules during the adsorption process (Hua *et al.* 2019). At $\text{pH} 9.0$, the MB adsorption capacity was observed to be 22.8 mg/g while a higher value of 23.5 mg/g was determined at $\text{pH} 7.0$, implying that pH adjustment was unnecessary.

The effects of RCM dosages on adsorption capacity and removal efficiency of MB in solution (20 mL, 100 ppm) were further studied by varying the amount of RCMs added (10 to 200 mg) at 20 °C for 3 h. As shown in Fig. 4b, the adsorption capacity (q_e) of the RCMs slightly increased when the RCM dosage was initially increased from 10 to 20 mg, and then q_e decreased because of unsaturated dye adsorption at higher sorbent dosages. In contrast, the removal efficiency for MB continuously increased with increasing of the sorbent dosage, finally yielding a removal ratio of 95.0% using 200 mg RCMs.

The effect of temperature on adsorption capacity of MB in solution (20 mL, 100 ppm, and 40 mg of RCMs) was investigated by increasing the temperature from 20 to 60 °C for 3 h (Fig. 4c). The adsorption capacity of the RCMs continuously decreased under the adopted conditions, indicating that a higher adsorption temperature resulted in

desorption of MB from the RCMs. For a high adsorption capacity and good removal efficiency for MB, the RCM dosage of 40 mg, temperature of 20 °C, and pH 7.0 were deduced as optimal to conduct further adsorption experiments.

Figure 4d presents the adsorption kinetics of the RCMs at an initial MB concentration of 100 ppm. The adsorption was rapid in the first 15 min, and then it remained constant after 1 h. In contrast, cellulose aerogel beads with a larger particle size exhibited a similar equilibrium adsorption capacity and a longer adsorption time (~2 h) under similar adsorption conditions (Hua *et al.* 2019). The reasons for the rapid adsorption are: (1) the smaller size and higher surface area of RCMs, which considerably increase contact area for the MB molecules, thus capturing them, and (2) the abundant micro/nanoporous structures in RCMs, which greatly improve the diffusion of MB molecules. When the adsorption equilibrium was reached, the MB adsorption capacity of the RCMs was up to 24.5 mg/g.

Pseudo-first- and pseudo-second-order models were used to elucidate the adsorption kinetics of MB molecules, and the corresponding adsorption data were calculated and fitted to the models (Fig. 4e and Table 2). The results suggested that the pseudo-second-order model was a better fit for the data than the pseudo-first-order model based on the R^2 value. Hubbe *et al.* (2019) pointed out that the good fits of adsorption rate data to the model could be explained by the diffusion mechanism. Here, the intra-particle diffusion model was chosen to evaluate the diffusion mechanism of MB in its adsorption process (Fig. 4f). It was evident that diffusion mechanism can be attributed to a relatively fast process at low times to diffusion from the bulk of solution to the RCM surface, a slow process to diffusion within the cellulose gel, and dynamic adsorption-desorption equilibrium in the RCM (Tang *et al.* 2019). These results indicated that the adsorption of MB onto the RCMs was controlled by external diffusion and adsorption. Thus, the RCM aerogel exhibited fast and efficient adsorption characteristics. Overall, the electrostatic interaction was the main adsorptive forces for the MB adsorption.

Three well-known adsorption isotherm models including Langmuir, Freundlich, and Temkin models, were adopted to further explore the adsorption capacity of MB on RCMs and interactive feature between the RCMs and MB. As shown in Fig. 4g and h, the equilibrium adsorption capacity increased rapidly at low equilibrium concentration of MB solution (< 21 ppm). Then it further increased a maximum adsorption capacity of 24.6 mg/g for RCMs at the high initial concentration of MB solution (200 ppm). Additionally, the corresponding parameters of the fittings for three adsorption isotherm models are calculated and listed in Table 3. The fitting results revealed that the Langmuir isothermal model better described the adsorption behavior than Freundlich and Temkin model, implying the monolayer adsorption of MB on the surface and the bulk of RCMs (Chen *et al.* 2017). The maximum adsorption capacity (q_m) calculated via the Langmuir model was 25.5 mg/g and similar to measured adsorption capacity (24.6 mg/g). The maximum adsorption capacities of sorbents, such as cellulose aerogel beads and some natural materials including zeolite, orange peel, and carboxymethyl cellulose beads are listed in Table 4. The higher adsorption capacity of RCMs was obtained compared to aforementioned cellulose-based or other materials, even though some difference in the inherent nature of adsorbents and adsorption conditions existed, suggesting that cellulose microspheres was considered as a promising sorbent for the efficient removal of MB from wastewater.

In addition to the high adsorption capacity, good recyclability of the microspheres is crucial for their sustainability and practicability. Ten cycles of the adsorption-desorption

process were performed to estimate the regeneration performance of the RCMs. HCl (0.1 M) was used to remove MB from the RCMs during the desorption process. As shown in Fig. 4i, even though a decrease was observed in the removal rate of MB from the solution during the ten regeneration cycles, the removal rate was maintained at approximately 70.0%, which could be ascribed to the structural stability of the RCMs. The good regeneration properties, as well as the high removal capacity and efficiency of RCMs, make them ideal candidates for both laboratory and industrial practical applications in the separation and purification of wastewater.

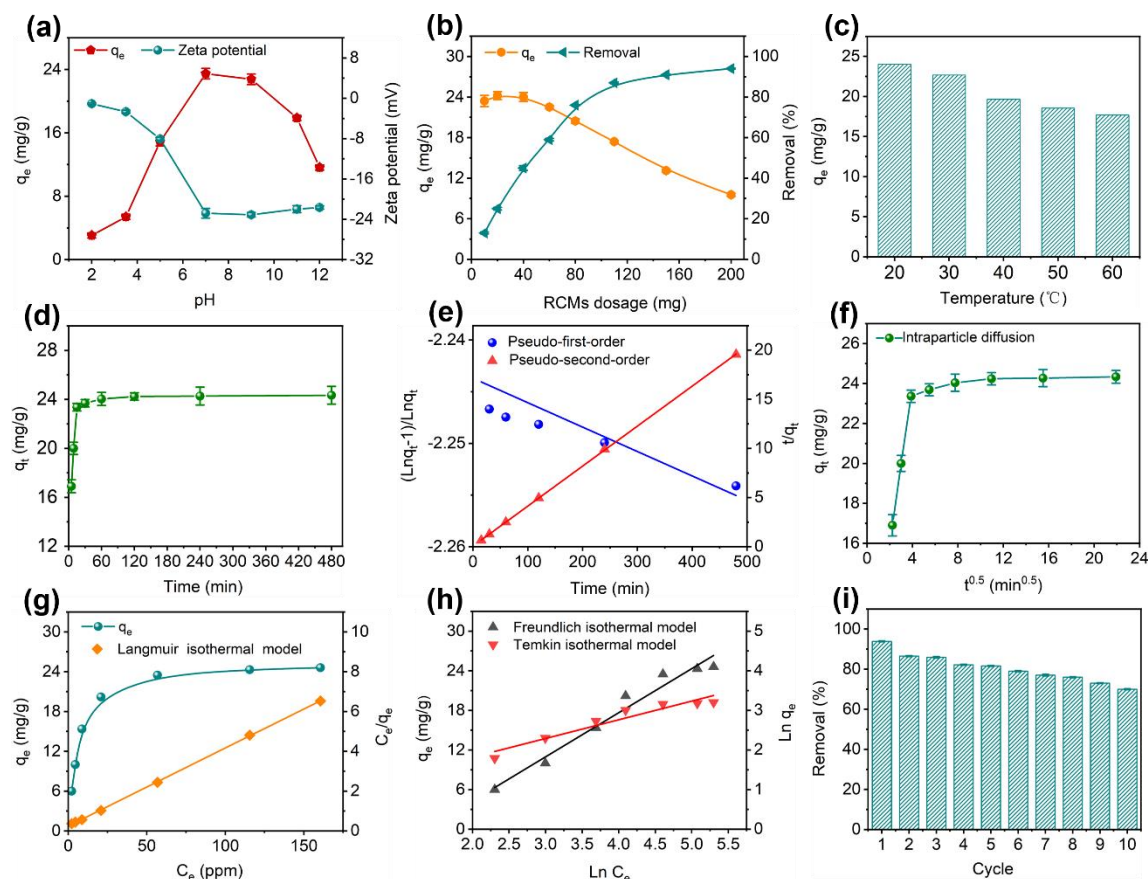


Fig. 4. (a) Effect of initial pH of MB solution on the adsorption capacity (q_e) and zeta potential. (b) Effect of adsorbent dosage on the q_e and removal of MB in the solution. (c) Effect of adsorption temperature on q_e . (d) Adsorption kinetics of RCMs in 100 ppm MB solution. (e) The data fitted to Pseudo-first-order and Pseudo-second-order models. (f) The data fitted to intraparticle diffusion model. (g) Adsorption isotherm of RCMs and the data fitted with Langmuir isotherm model. (h) The data fitted with the Freundlich and Temkin isotherm model. (i) The adsorption performance of the regenerated RCMs

Table 2. Parameters of Pseudo-first-order, Pseudo-second-order and Intra Particle Diffusion for RCMs Adsorption Kinetics

Pseudo-First-Order		Pseudo-Second-Order	
k_1	R^2	k_2	R^2
0.0135	0.953	0.0236	0.999

Table 3. Langmuir, Freundlich, and Temkin Constants of RCMs for MB Adsorption

Sample	Langmuir Isotherm			Freundlich Isotherm			Temkin Isotherm		
	q_m	K_L	R^2	K_F	n	R^2	A	B	R^2
RCMs	25.5	0.03	0.999	2.40	2.12	0.924	6.63	0.26	0.965

Table 4. Maximum Adsorption Capacities of the Reported Sorbents and RCMs for MB

Materials	q_m (mg/g)	References
Orange peel	18.6	Annadurai <i>et al.</i> (2002)
Wheat straw	16.2	Batzias <i>et al.</i> (2009)
Zeolite	23.7	Sun <i>et al.</i> (2010)
Alginate/almond peanut biocomposite	22.8	Erfani and Javanbakht (2018)
Carboxymethyl cellulose beads	12.5	Liu <i>et al.</i> (2018)
Magnetic chitosan beads	20.4	Rahmi <i>et al.</i> (2019)
Calcium alginate biobeads	23.0	Hachi <i>et al.</i> (2016)
RCMs	24.5	This work

CONCLUSIONS

1. In this work, porous regenerated cellulose microspheres (RCMs) were synthesized for adsorption of methylene blue using a simple emulsification–acid coagulation–oven-drying technique after dissolving cellulose in tetraethylammonium hydroxide (TEAOH)/urea solvents at room temperature.
2. The viscosities of cellulose solution (~ 2.0 wt%) notably decreased when storage time was extended from 2 h to 10 days owing to the decrease in cellulose degree of polymerization (DP), which implied that the cellulose was degraded in the TEAOH/urea solvent. However, the surface tension of cellulose solution and the particle size of the RCMs were not significantly influenced by the storage time of cellulose solution.
3. Porous RCMs possessing cellulose II structure, high DP (1000), small mean size (20 to 224 μm), good swelling properties (8.27 to 10.23 g/g) and chemical/thermal stabilities were prepared by controlling the surfactant (polysorbate 80) dosage in the range 2 to 8 wt%. Increasing the surfactant dosage resulted in a notably reduced particle sizes of the RCMs.
4. Pure RCMs without chemical modification exhibited rapid adsorption (~1 h to reach equilibrium) and high MB adsorption capacity (24.5 mg/g) under the optimal conditions. The RCMs could be regenerated and reused several times, thereby validating their potential for adsorption of cationic MB.

ACKNOWLEDGMENTS

This research is financially supported by Basic Science Research Program through the National Research Foundation of Korea (NRF) funded by the Ministry of Education (NRF-2019R1A2C2009284).

REFERENCES CITED

- Abe, M., Fukaya, Y., and Ohno, H. (2012). "Fast and facile dissolution of cellulose with tetrabutylphosphonium hydroxide containing 40 wt% water," *Chem. Commun.* 48, 1808-1810. DOI: 10.1039/c2cc16203b
- Adsul, M., Soni, S. K., Bhargava, S. K., and Bansal, V. (2012). "Facile approach for the dispersion of regenerated cellulose in aqueous system in the form of nanoparticles," *Biomacromolecules*. 13, 2890-2895. DOI: 10.1021/bm3009022
- Annadurai, G., Juang, R.-S., and Lee, D.-J. (2002). "Use of cellulose-based wastes for adsorption of dyes from aqueous solutions," *J. Hazard. Mater.* B92, 263-274. DOI: 10.1016/s0304-3894(02)00017-1
- Batzias, F., Sidiras, D., Schroeder, E., and Weber, C. (2009). "Simulation of dye adsorption on hydrolyzed wheat straw in batch and fixed-bed systems," *Chem. Eng. J.* 148, 459-472. DOI:10.1016/j.cej.2008.09.025
- Buchtova, N., Pradille, C., Bouvard, J. L., and Budtova, T. (2019). "Mechanical properties of cellulose aerogels and cryogels," *Soft Matter*. 15, 7901-7908. DOI: 10.1039/c9sm01028a
- Chen, P., Liu, X., Jin, R., Nie, W., and Zhou, Y. (2017). "Dye adsorption and photo-induced recycling of hydroxypropyl cellulose/molybdenum disulfide composite hydrogels," *Carbohydr. Polym.* 167, 36-43. DOI: 10.1016/j.carbpol.2017.02.094
- Dong, J., Zeng, J., Wang, B., Cheng, Z., Xu, J., Gao, W., and Chen, K. (2021). "Mechanically flexible carbon aerogel with wavy layers and springboard elastic supporting structure for selective oil/organic solvent recovery. *ACS Appl. Mater. Interfaces*. 13, 15910-15924. DOI: 10.1021/acsami.1c02394
- Druel, L., Niemeyer, P., Milow, B., and Budtova, T. (2018). "Rheology of cellulose-[DBNH][CO₂Et] solutions and shaping into aerogel beads," *Green Chem.* 20, 3993-4002. DOI: 10.1039/C8GC01189C
- Druel, L., Kenkel, A., Baudron, V., Buwalda, S., and Budtova, T. (2020). "Cellulose aerogel microparticles via emulsion-coagulation technique," *Biomacromolecules*. 21, 1824-1831. DOI: 10.1021/acs.biomac.9b01725
- Erfani, M., and Javanbakht, V. (2018). "Methylene Blue removal from aqueous solution by a biocomposite synthesized from sodium alginate and wastes of oil extraction from almond peanut," *Int. J. Biol. Macromol.* 114, 244-255. DOI: 10.1016/j.ijbiomac.2018.03.003
- Gericke, M., Trygg, J., and Fardim, P. (2013). "Functional cellulose beads: Preparation, characterization, and applications," *Chem. Rev.* 113, 4812-4836. DOI: 10.1021/cr300242j
- Hachi, M., Chergui, A., Selatnia, A., and Cabana, H. (2016). "Valorization of the spent biomass of pleurotus mutilus immobilized as calcium alginate biobeads for methylene blue biosorption," *Environ. Process.* 3, 413-430. DOI: 10.1007/s40710-016-0157-z
- Hua, J., Meng, R., Wang, T., Gao, H., Luo, Z., Jin, Y., Liu, L., and Yao, J. (2019).

- "Highly porous cellulose microbeads and their adsorption for methylene blue," *Fibers Polym.* 20, 794-803. DOI: 10.1007/s12221-019-8334-0
- Hubbe, M. A., Azizian, S., and Douven, S. (2019). "Implications of apparent pseudo-second-order adsorption kinetics onto cellulosic materials. A review," *BioResources* 14(3), 7582-7626. DOI: 10.15376/biores.14.3.7582-7626
- Kim, Y., An, H.-J., and Cho, B.-U. (2020). "Production of cellulose beads with TEAH-urea solvent and dropping technique: Effect of inner diameter of syringe needle," *J. Korea TAPPI.* 52, 149-156. DOI: 10.7584/JKTAPPI.2020.12.52.6.149
- Kim, Y., An, H.-J., and Cho, B.-U. (2021). "Production of cellulose beads with tetraethylammonium hydroxideurea solvent and dropping technique: Effect of concentration of cellulose solution," *J. Korea TAPPI.* 53, 83-89. DOI: 10.7584/JKTAPPI.2021.02.53.1.83
- Lapwanit, S., Sooksimuang, T., and Trakulsujaritchok, T. (2018). "Adsorptive removal of cationic methylene blue dye by kappa-carrageenan/poly(glycidyl methacrylate) hydrogel beads: Preparation and characterization," *J. Environ. Chem. Eng.* 6, 6221-6230. DOI: 10.1016/j.jece.2018.09.050
- Li, Z., Sellaoui, L., Franco, D., Netto, M. S., Georgin, J., Dotto, G. L., Bajahzar, A., Belmabrouk, H., Bonilla-Petriciolet, A., and Li, Q. (2020). "Adsorption of hazardous dyes on functionalized multiwalled carbon nanotubes in single and binary systems: Experimental study and physicochemical interpretation of the adsorption mechanism," *Chem. Eng. J.* 389, 124467. DOI: 10.1016/j.cej.2020.124467
- Li, W., Luo, X., Song, R., Zhu, Y., Li, B., and Liu, S. (2016). "Porous cellulose microgel particle: A fascinating host for the encapsulation, protection, and delivery of *Lactobacillus plantarum*," *J. Agr. Food Chem.* 64, 3430-3436. DOI: 10.1021/acs.jafc.6b00481
- Liu, C., Omer, A. M., and Ouyang, X. K. (2018). "Adsorptive removal of cationic methylene blue dye using carboxymethyl cellulose/k-carrageenan/activated montmorillonite composite beads: Isotherm and kinetic studies," *Int. J. Biol. Macromol.* 106, 823-833. DOI: 10.1016/j.ijbiomac.2017.08.084
- Liu, X., Tian, J., Li, Y., Sun, N., Mi, S., Xie, Y., and Chen, Z. (2019). "Enhanced dyes adsorption from wastewater via Fe₃O₄ nanoparticles functionalized activated carbon," *J. Hazard. Mater.* 373, 397-407. DOI: 10.1016/j.jhazmat.2019.03.103
- Luo, X., and Zhang, L. (2010). "Creation of regenerated cellulose microspheres with diameter ranging from micron to millimeter for chromatography applications," *J. Chromatogr. A.* 1217, 5922-5929. DOI: 10.1016/j.chroma.2010.07.026
- Lu, X., and Shen, X. (2011). "Solubility of bacteria cellulose in zinc chloride aqueous solutions," *Carbohydr. Polym.* 86, 239-244. DOI: 10.1016/j.carbpol.2011.04.042
- Molla, A., Li, Y., Mandal, B., Kang, S. G., Hur, S. H., and Chung, J. S. (2018). "Selective adsorption of organic dyes on graphene oxide: Theoretical and experimental analysis," *Appl. Surf. Sci.* 464, 170-177. DOI: 10.1016/j.apsusc.2018.09.056
- Peng, F., Ren, J.-L., Xu, F., Bian, J., Peng, P., and Sun, R.-C. (2009). "Comparative study of hemicelluloses obtained by graded ethanol precipitation from sugarcane bagasse," *J. Agric. Food Chem.* 57, 6305-6317. DOI: 10.1021/jf900986b
- Qin, X., Lu, A., and Zhang, L. (2009). "Gelation behavior of cellulose in NaOH/urea aqueous system via cross-linking," *Cellulose.* 20, 1669-1677. DOI: 10.1007/s10570-013-9961-z
- Rahmi, Ishmaturrehmi, and Mustafa, I. (2019). "Methylene blue removal from water

- using H₂SO₄ crosslinked magnetic chitosan nanocomposite beads," *Microchem. J.* 144, 397-402. DOI: 10.1016/j.microc.2018.09.032
- Saito, T., and Isogai, A. (2004). "TEMPO-mediated oxidation of native cellulose. The effect of oxidation conditions on chemical and crystal structures of the water-insoluble fractions," *Biomacromolecules* 5, 1983-1989. DOI: 10.1021/bm0497769
- Sirviö, J. A., and Heiskanen, J. P. (2019). "Room-temperature dissolution and chemical modification of cellulose in aqueous tetraethylammonium hydroxide-carbamide solutions," *Cellulose* 27, 1933-1950. DOI: 10.1007/s10570-019-02907-x
- Sun, Z., Li, C., and Wu, D. (2010). "Removal of methylene blue from aqueous solution by adsorption onto zeolite synthesized from coal fly ash and its thermal regeneration," *J. Chem. Technol. Biot.* 85, 845-850. DOI: 10.1002/jctb.2377
- Suzuki, T., Kono, K., Shimomura, K., and Minami, H. (2014). "Preparation of cellulose particles using an ionic liquid," *J. Colloid Interface Sci.* 418, 126-131. DOI: 10.1016/j.jcis.2013.12.014
- Tang, J., Song, Y., Zhao, F., Spinney, S., Bernardes, J. S., and Tam, K. C. (2019). "Compressible cellulose nanofibril (CNF) based aerogels produced via a bio-inspired strategy for heavy metal ion and dye removal," *Carbohydr. Polym.* 208, 404-412. DOI: 10.1016/j.carbpol.2018.12.079
- Tang, X., Wang, T., Zhang, S., Fang, L., and Zheng, H. (2021). "Enhanced performance of a novel flocculant containing rich fluorine groups in refractory dyeing wastewater treatment: Removal mechanisms," *Sep. Purif. Technol.* 263, article 118411. DOI: 10.1016/j.seppur.2021.118411
- Tu, H., Zhu, M., Duan, B., and Zhang, L. (2021). "Recent progress in high-strength and robust regenerated cellulose materials," *Adv. Mater.* 33, article 2000682. DOI: 10.1002/adma.202000682
- Wang, Q., Fu, A., Li, H., Liu, J., Guo, P., Zhao, X. S., and Xia, L.H. (2014). "Preparation of cellulose based microspheres by combining spray coagulating with spray drying," *Carbohydr. Polym.* 111, 393-399. DOI: 10.1016/j.carbpol.2014.05.002
- Wei, W., Meng, F., Cui, Y., Jiang, M., and Zhou, Z. (2016). "Room temperature dissolution of cellulose in tetra-butylammonium hydroxide aqueous solvent through adjustment of solvent amphiphilicity," *Cellulose*. 24, 49-59. DOI: 10.1007/s10570-016-1113-9
- Xu, F., and Cho, B.-U. (2022). "Preparation of porous regenerated cellulose microstructures via emulsion-coagulation technique," *Cellulose*. 29, 1527-1542. DOI: 10.1007/s10570-022-04428-6
- Xie, J., Xu, J., Cheng, Z., Chen, J., Zhang, Z., Chen, T., Yang, R., and Sheng, J. (2020). "Facile synthesis of fluorine-free cellulosic paper with excellent oil and grease resistance," *Cellulose*. 7, 7009-7022. DOI: 10.1007/s10570-020-03248-w.
- Zhang, J., Wang, M., Li, W., Wei, W., Li, J., Jiang, M., Wang, Y., and Zhou, Z. (2019). "TBAH/Urea/H₂O solvent for room temperature wet-spinning of cellulose and optimization of drawing process," *Cellulose*. 26, 6959-6977. DOI: 10.1007/s10570-019-02536-4

Article submitted: September 8, 2022; Peer review completed: November 1, 2022;

Revised version received: November 15, 2022; Further revised version received and accepted: November 20, 2022; Published: November 30, 2022.

DOI: 10.15376/biores.18.1.748-766

APPENDIX

Supplemental Material

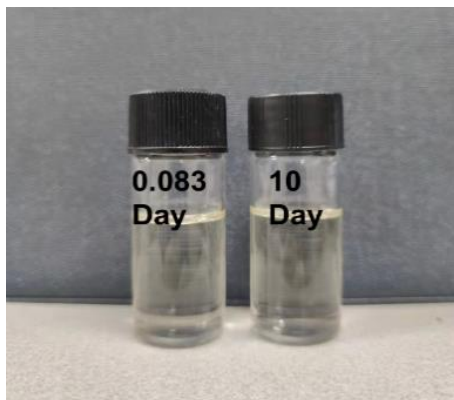


Fig. S1. Images of obtained cellulose solution at 0.083 day (left) and 10 days (right)

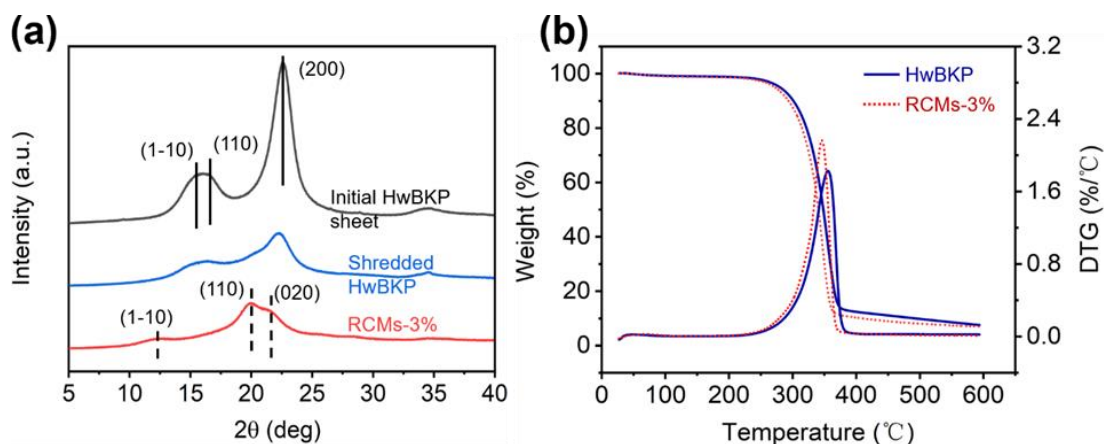


Fig. S2. (a) XRD spectra; (b) TG and DTG curves of S-HwBKP and RCMs

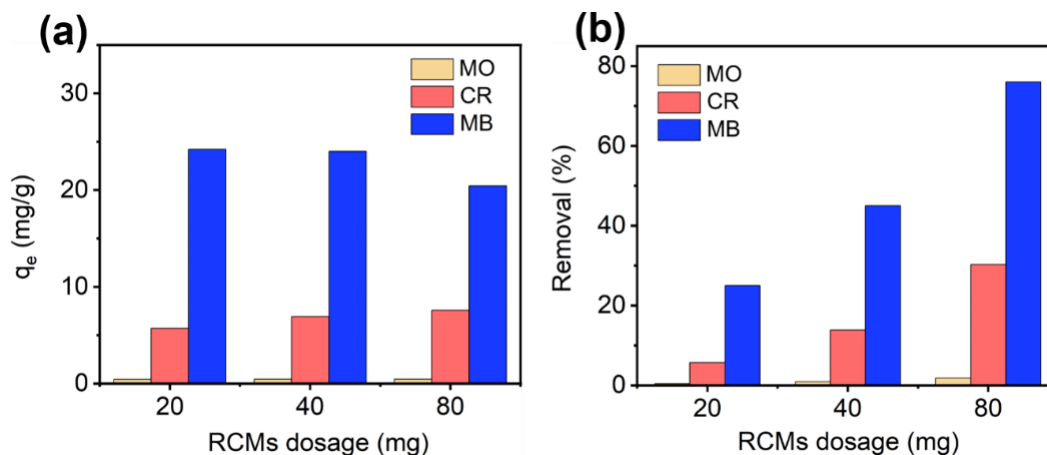


Fig. S3. Effect of absorbent dosage on (a) q_e and (b) removal of methyl orange (MO), Congo red (CR) and methylene blue (MB) in the solution

Table S1. Chemical Components of S-HwBKP and RCMs-3% (%)

Sample	Holocellulose	1% NaOH solubility	Carboxyl groups ^a	α -cellulose	Lignin	Ash	Total ^b
S-HwBKP	98.21 \pm 0.32	3.70 \pm 0.50	0.09 \pm 0.01	90.15 \pm 0.15	0.95 \pm 0.02	0.30 \pm 0.02	99.46 \pm 0.04
RCMs	99.10 \pm 0.12	2.09 \pm 0.12	0.07 \pm 0.01	94.60 \pm 0.20	0.65 \pm 0.03	0.11 \pm 0.01	99.85 \pm 0.02

^a unit is mmol/g^b sum of holocellulose, lignin, and ash